

# Study of visible-light emission in pure and methane-doped liquid argon

---

**A. Bondar,<sup>a,b</sup> E. Borisova,<sup>a,b</sup> A. Buzulutskov,<sup>a,b</sup> E. Frolov,<sup>a,b</sup> V. Nosov,<sup>a,b</sup> V. Oleynikov,<sup>a,b,1</sup>  
A. Sokolov<sup>a,b</sup>**

<sup>a</sup>*Budker Institute of Nuclear Physics, Lavrentiev ave. 11, Novosibirsk 630090, Russia*

<sup>b</sup>*Novosibirsk State University, Pirogova st. 2, Novosibirsk 630090, Russia*

*E-mail:* [A.F.Buzulutskov@inp.nsk.su](mailto:A.F.Buzulutskov@inp.nsk.su), [V.P.Oleynikov@inp.nsk.su](mailto:V.P.Oleynikov@inp.nsk.su)

**ABSTRACT:** In liquid argon TPCs for dark matter search and neutrino detection experiments, primary scintillation light is used as a prompt signal of particle scattering, being intensively produced in the vacuum ultraviolet (VUV) due to excimer emission mechanism. On the other hand, there were indications on the production of visible-light emission in liquid argon, albeit at a much lower intensity, the origin of which is still not clear. The closely related issue is visible-light emission in liquid argon doped with methane, the interest in which is due to the possible use in neutron veto detectors for those experiments. In this work we study in detail the properties of such light emission in pure liquid argon and its mixtures with methane. In particular, the absolute photon yield of visible-light emission in pure liquid argon was measured to be about 200 and 90 photon/MeV for X-rays and alpha particles respectively. In liquid argon doped with methane the photon yield dropped down significantly, by about an order of magnitude at a methane molar content varying from 0.01 to 1%, and then almost did not change when further increasing the methane content up to 10%.

**KEYWORDS:** Noble liquid detectors (scintillation, ionization, double-phase); Dark Matter detectors (WIMPs, axions, etc.)

---

<sup>1</sup>Corresponding author.

---

## Contents

<b>1</b>	<b>Introduction</b>	<b>1</b>
<b>2</b>	<b>Experimental setup</b>	<b>3</b>
<b>3</b>	<b>Measurements with pure liquid argon</b>	<b>6</b>
3.1	Pulse-shape analysis	6
3.2	Photoelectron yield dependence on the drift field	7
3.3	Energy deposition	8
3.4	Absolute visible light yield	9
3.5	Comparison with the previous results	10
<b>4</b>	<b>Measurements with liquid argon doped with methane</b>	<b>12</b>
4.1	Pulse-shape analysis	12
4.2	Photoelectron and light yields	13
<b>5</b>	<b>Conclusions</b>	<b>16</b>
<b>A</b>	<b>Doping liquid argon with methane: drift velocity and charge yield</b>	<b>17</b>

---

## 1 Introduction

In liquid Ar TPCs for dark matter search [1] and neutrino detection [2] experiments, the scattered particle produces two types of signals: that of primary scintillation recorded promptly (“S1”) and that of primary ionization recorded with a delay (“S2”). The S2 signal is recorded typically indirectly in the gas phase of two-phase detectors [3] using the effect of proportional electroluminescence [4]. In contrast, the S1 signal is recorded directly using either photomultiplier tubes (PMTs) or silicon photomultipliers (SiPMs).

“Ordinary” primary scintillation light in liquid Ar forms from the excimer ( $\text{Ar}_2^*$ ) emission mechanism [1, 3, 5]. Scintillation light is intensely produced in the vacuum ultraviolet (VUV), around 128 nm, with a photon yield of about  $40 \times 10^3$  photon/MeV [3], and thus require a wavelength shifter (WLS), such as tetraphenyl-butadiene (TPB), to convert the VUV to the visible light suitable for detection with PMTs and SiPMs.

On the other hand, there were indications on light emission in the visible and near infrared (NIR) range in liquid Ar in S1 signal [6–14], albeit at a much lower yield, of the order of 500 photon/MeV [6], the origin of which is still not clear.

It was suggested in ref. [15] that such visible-light emission in liquid Ar might be explained by neutral bremsstrahlung (NBrS) of primary ionization electrons, decelerated in the medium down

to the energy domain of the NBrS effect (1-10 eV). The NBrS effect is that of bremsstrahlung of electrons scattered on neutral atoms [15]:

$$e^- + A \rightarrow e^- + A + h\nu . \quad (1.1)$$

So far, the NBrS emission in the form of electroluminescence in noble gases has been experimentally and theoretically studied in refs. [15–21] and [15, 22–24] respectively, with predicted continuous spectrum in the visible and NIR range.

The NBrS emission in single collision is naturally fast as it is defined by time of flight of the electron (of 1-10 eV kinetic energy) nearby the atom, which is of the order of  $10^{-4}$  ps. Since to reduce the electron energy from 10 to 1 eV it takes about  $10^5$  collisions, with electron mean free path between them of about 10 nm and electron velocity of about  $10^6$  m/s, the overall time of the NBrS emission from primary ionization electrons would be of the order of 1 ns.

Also it is known that electroluminescence in the VUV in gaseous Ar due to the excimer effect is associated with primary scintillation VUV light in liquid Ar due to the same excimer effect. Similarly, one could assume that the visible-light emission due to the NBrS effect would exist both in gaseous and liquid Ar.

The closely related issue is visible-light emission in liquid Ar doped with  $\text{CH}_4$ , the interest in which is due to the possible use in neutron veto detectors for dark matter search experiments. To achieve a high efficiency of neutron detection, the working medium of the veto detector should contain hydrogen, acting as a neutron moderator. So far, neutron veto detectors based on flammable mixtures of liquid organic scintillators have been used [25, 26]. A safe alternative might be a liquid scintillator based on liquid Ar doped with  $\text{CH}_4$ . This idea was discussed for application in the DarkSide experiment [27]. In particular, the  $\text{CH}_4$  content of 5-10% in liquid Ar would be enough for compact neutron veto detector of about 1 m thick.

However, it is well known that even tiny amount ( $>0.1$  ppm) of  $\text{CH}_4$  dopant would immediately quench excimer scintillations in liquid Ar [28]. The quenching is due to both VUV light absorption on  $\text{CH}_4$  [28, 29] and excimer deexcitation in collisions with  $\text{CH}_4$  molecules. On the other hand, this may not be the case for visible-light emission due to the NBrS effect: it can be expected not to be suppressed by the  $\text{CH}_4$  dopant. Indeed, the NBrS radiation induced by primary ionization electrons was supposed to be present not only in atomic noble gases, but in molecular gases as well, namely in air [30]. Similarly, we may suppose that the NBrS emission could also exist in a liquid mixture of Ar and  $\text{CH}_4$  in the form of light emission in the visible and NIR range.

Accordingly, in this work we systematically study the properties of visible-light emission of S1 signal both in pure liquid Ar and its mixtures with  $\text{CH}_4$  to verify the previous results and hypotheses. The preliminary results of the study were published in ref. [14]. In the current work, the experimental setup design was improved compared to that of ref. [14], namely photon collection efficiency was increased, cross-talk background was decreased and an alpha-particle source of irradiation was used in addition to that of pulsed X-ray. As a result, the photon yields of visible-light emission were measured in pure liquid Ar and its mixtures with  $\text{CH}_4$  with improved accuracy. The relevance of the results obtained to the development of noble liquid detectors for dark matter searches is also discussed.



In measurements with pure Ar the  $N_2$  content was below 1 ppm (with the measurement accuracy of 1 ppm); it was monitored before and after measurement session using an ‘‘SVET’’ gas analyzer [33], which employed emission-spectrum-measurement technique.

The cryogenic chamber operated in the single-phase mode was composed of two gaps: that of drift (with low electric field, namely drift field  $F_d$ ), 48 mm thick, and that of induction (with high electric field,  $F_i$ ), 22 mm thick. To form these gaps, the electrodes made from THGEMs (Thick Gas Electron Multipliers, [34]) were used: see Fig. 1. The drift gap was formed by a cathode electrode, field-shaping electrodes and THGEM0. The induction gap was formed by THGEM0 and THGEM1, the latter acting as an anode. In the two-phase mode the induction gap was divided into two: that of extraction (with high electric field,  $F_{extr}$ ), 9 mm thick, located between THGEM0 and liquid level, and that of electroluminescence (with high electric field,  $F_{EL}$ ), 13 mm thick, located between the liquid level and THGEM1. The liquid level was calculated from the amount of condensed Ar using CAD software and was verified using THGEM1 as a capacitive liquid level meter.

Two different types of spectral devices were used in the measurements. Four compact cryogenic PMTs R6041-506MOD [35] were located on the perimeter of the induction (or extraction/electroluminescence) gap and electrically insulated from it by an acrylic box. Another spectral device was a  $5 \times 5$  SiPM matrix, composed from SiPMs of MPPCs 13360-6050PE type [36] with an active area of  $6 \times 6 \text{ mm}^2$  each and channel pitch of 1 cm. The PMTs and SiPM matrix were protected from the TPC electric fields using grounded metal meshes in front of them. The independence of their gain characteristics from the electric field was confirmed in experiment.

Fig. 2 (top) shows the spectral characteristics of the detector, namely the Photon Detection Efficiency (PDE) of SiPMs, Quantum Efficiency (QE) of PMTs, transmittance of the UV and ordinary acrylic plate in front of the PMTs and SiPM matrix, respectively. Taking into account the transmission of the acrylic plates, the PMTs and SiPM matrix were sensitive in the range of 270-650 nm and 360-1000 nm, respectively. The spectral devices were insensitive to the VUV, since no WLS was used in the experimental setup.

For comparison, Fig. 2 (bottom) shows the emission spectra in the visible range in pure liquid Ar, measured in Heindl et al. [10] and Auger et al. [12] for light emission of S1 signal and electroluminescence respectively. We also show the spectrum of electroluminescence in liquid Ar due to the NBrS EL effect, theoretically calculated in ref. [23] for the electric field of 200 kV/cm, the latter roughly corresponding to the maximum field used in Auger et al. [12]. One can see that all the spectra are rather flat. Also, both the SiPM matrix and PMTs were sensitive to all of them.

The detector was irradiated from outside by X-rays from a pulsed X-ray tube with Mo anode, with the average deposited energy in liquid Ar of 25 keV [39], or by alpha particles with the energy of 5.5 MeV from a  $^{238}\text{Pu}$  source with an activity of about  $5 \times 10^4$  Bq, installed at the center of the cathode inside the detector.

The signals from the PMTs were amplified using fast 10-fold amplifiers CAEN N979 and linear amplifiers with a shaping time of 10 and 200 ns respectively. The signals from SiPMs were transmitted to fast amplifiers with a shaping time of 40 ns, via twisted pair wires. The charge signal from the THGEM1 anode was recorded using a calibrated chain of a preamplifier and shaping amplifier. All amplifiers were placed outside the detector.

The DAQ system included both a 4-channel oscilloscope LeCroy WR HRO 66Zi and a 64-channel Flash ADC CAEN V1740 (12 bits, 62.5 MHz): the signals were digitized and stored

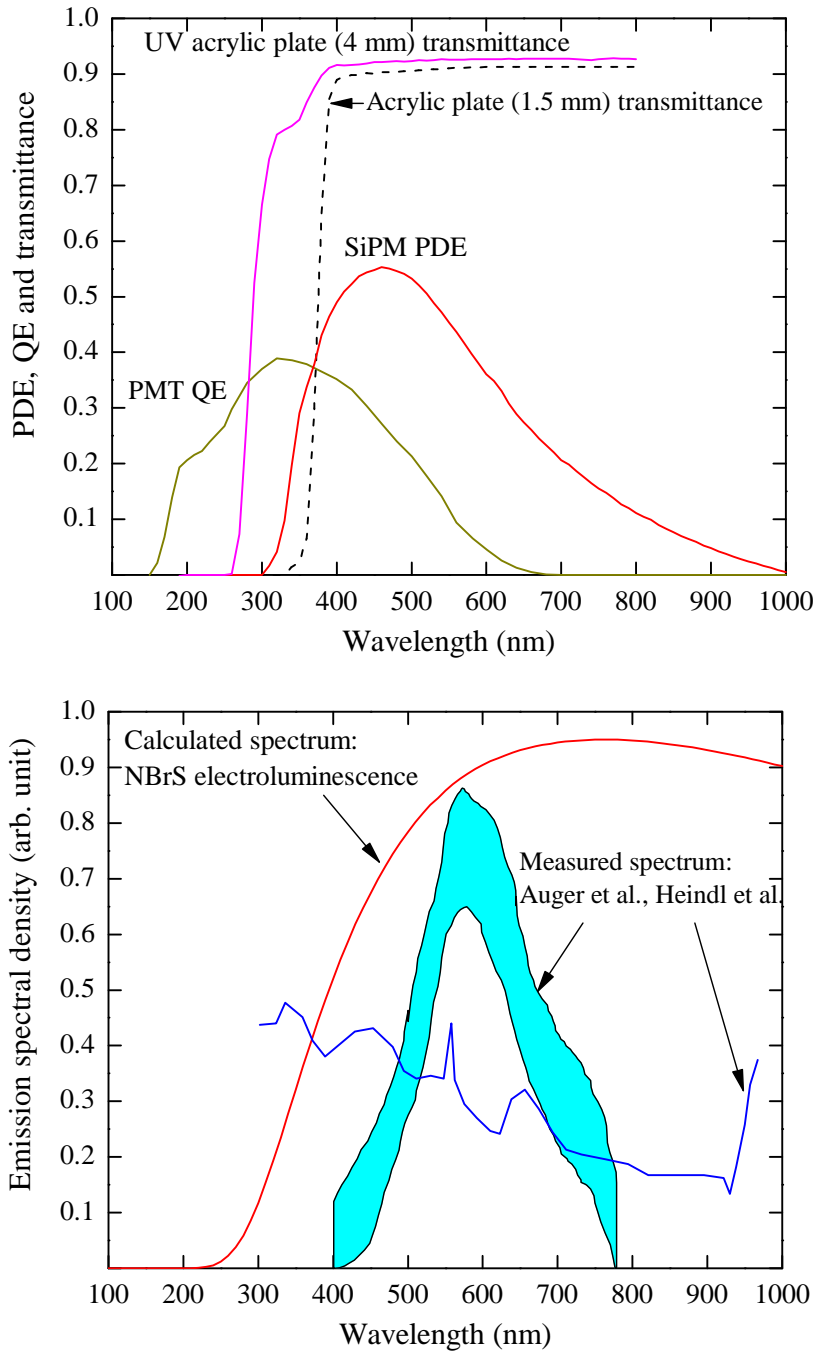


**Figure 2.** Top: Photon Detection Efficiency (PDE) of SiPM (MPPC 13360-6050PE [36]) at overvoltage of 5.6 V obtained from ref. [37] using the PDE voltage dependence, Quantum Efficiency (QE) of the PMT R6041-506MOD at 87 K obtained from refs. [36, 38] using a temperature dependence derived there, the transmittance of the UV and ordinary acrylic plate in front of the PMTs and SiPM matrix, respectively. Bottom: liquid Ar emission spectra measured in Heindl et al. [10] (light emission of S1 signal) and Auger et al. [12] (electroluminescence due to HV breakdown at  $\leq 200$  kV/cm), as well as electroluminescence spectrum due to the NBrS EL effect at 200 kV/cm theoretically calculated in ref. [23].

both in the oscilloscope and in a computer for further off-line analysis. In measurements with the pulsed X-ray tube, the trigger was provided by its pulse generator. In measurements with alpha particles, the trigger was provided by the S2 signal taken from all the PMTs, in this case the detector being operated in the two-phase mode: see Fig. 3. Note that at higher electric fields the electroluminescence (S2) signal had the characteristic slow component with time constant of about  $5 \mu\text{s}$ , similar to that observed elsewhere [40].

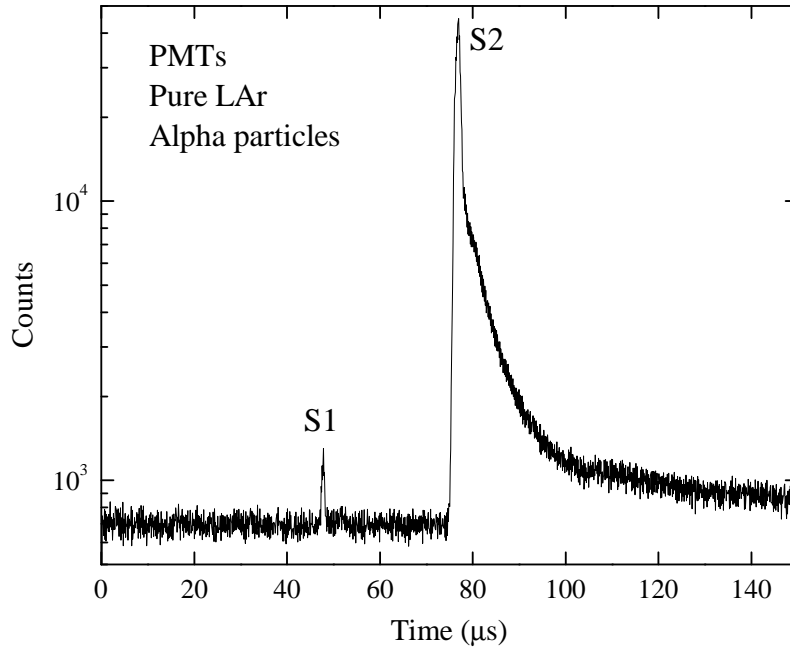


**Figure 3.** Pulse-shape of S1 and S2 signals, induced by alpha particles, obtained in the two-phase mode and recorded by PMTs. The data were obtained at the maximum electric field in pure liquid Ar ( $F_d = 0.62 \text{ kV/cm}$ ,  $F_{EL} = 7.8 \text{ kV/cm}$ ). The S2 signal amplitude significantly exceeded that of S1, which allowed to use the S2 signal as a trigger. Note that the S2 signal has the slow component with time constant of about  $5 \mu\text{s}$ , similar to that observed elsewhere [40].

### 3 Measurements with pure liquid argon

#### 3.1 Pulse-shape analysis

Pulse shape analysis can provide valuable information on the mechanisms of light emission in liquid Ar. Fig. 4 shows the averaged pulse shape of the S1 signal from PMTs and SiPM matrix, induced by alpha particles and pulsed X-rays, obtained in pure liquid Ar.

The S1 signal obtained with the pulsed X-ray tube had two distant peaks due to characteristic double-pulse structure of the X-ray tube itself, which was determined in special measurements using a BGO scintillation counter [7]. The peak width is defined by the X-ray pulse width, of about  $0.5 \mu\text{s}$  [7], from which one can estimate the time constants ( $\tau$ ) of visible-light emission themselves. In particular, one can deduce that visible-light emission in pure liquid Ar had the fast ( $\tau_f < 100 \text{ ns}$ ) and slow ( $\tau_s \sim 1 \mu\text{s}$ ) components of about the same contribution. On the other hand, the S1 signal

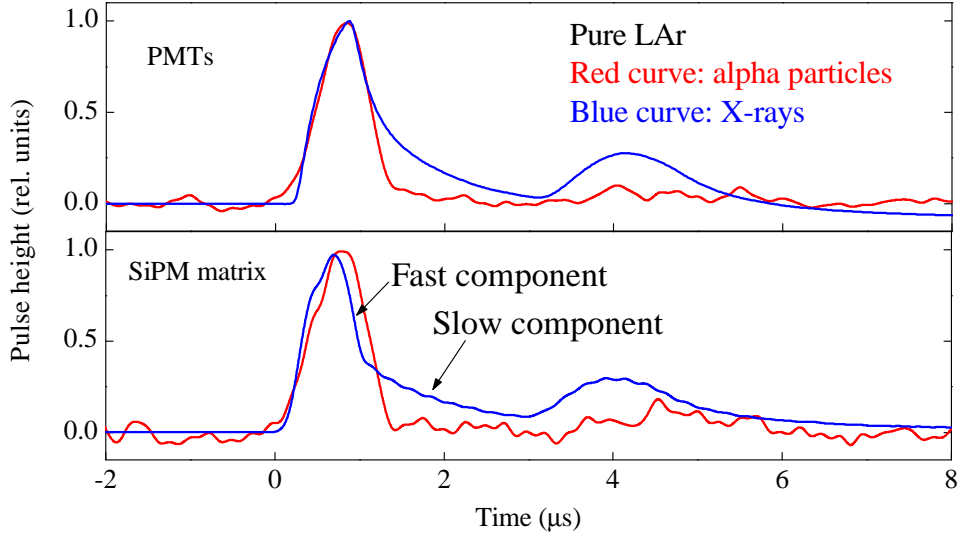


**Figure 4.** Averaged pulse shapes of the S1 signals, induced by alpha particles and pulsed X-rays, obtained in the two-phase mode in pure liquid Ar and recorded by SiPM matrix and PMTs. Data with pulsed X-rays and alpha particles were obtained at zero and maximum electric field ( $F_d = 0.62$  kV/cm,  $F_{EL} = 7.8$  kV/cm), respectively. All the pulse heights are normalized to the maximum.

obtained with the alpha particle source had the fast component only. Also, the S1 pulse shape did not depend on the electric field.

### 3.2 Photoelectron yield dependence on the drift field

Fig. 5 shows the photoelectron yield of visible-light emission in liquid Ar, expressed in the number of photoelectrons (photoelectron number) recorded by PMTs and SiPM matrix, as a function of the drift field. The photoelectron number was integrated over the time interval of  $10 \mu\text{s}$  from the beginning of the signal and normalized to that of zero electric field. One can see that the photoelectron yield of visible-light emission is almost independent of the drift field, in contrast to that of excimer (VUV) scintillations, the yield of which substantially decreases with the drift field, the latter being explained by weakening of the electron-ion recombination at higher electric fields [3].

This difference obviously indicates on the different mechanisms of visible-light emission and excimer scintillation in liquid Ar, in particular on that visible-light emission is not related to excited Ar states (the latter are copiously produced in electron-ion recombination). On the other hand, the light yield independence of the electric field is naturally explained in the frame of NBrS mechanism, where the photons are emitted due to elastic electron scattering on atoms (see Eq. 1.1).

It should be noted that a similar plot for alpha particles does not make much sense, because of the small statistics the photoelectrons number fluctuations are too large, of about 10%, i.e. of the order of the effect.

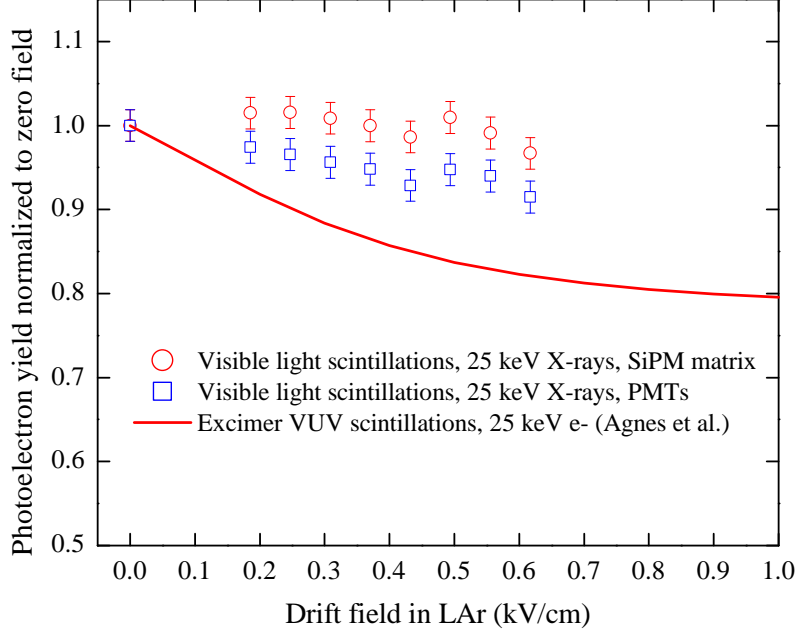


**Figure 5.** Relative photoelectron yield of visible-light emission of S1 signal in pure liquid Ar recorded by PMTs and SiPM matrix in single-phase mode, induced by pulsed X-rays with an average deposited energy of 25 keV, as a function of the electric field (data points). For comparison, the relative photoelectron yield of excimer (VUV) scintillations induced by electrons with an energy of 25 keV is shown, obtained from Agnes et al. [41] using the stopping power of electrons in Ar from ref. [42] (curve).

### 3.3 Energy deposition

To calculate the absolute photon yield of visible-light emission one need to know the energy deposited in liquid Ar. In measurements with alpha particles, one alpha particle was mainly recorded per event, resulting in that the deposited energy (5.5 MeV) was well defined. In measurements with pulsed X-rays, the detector recorded a large number of X-ray photons in each pulse and the energy deposition ( $E_{dep}$ ) can be determined using the following formula:

$$E_{dep} = N_i \cdot W, \quad (3.1)$$

where  $N_i$  is the primary ionization charge and  $W=23.6$  eV is the energy needed to produce one ion pair in liquid Ar [43].

The primary ionization charge ( $N_i$ ) was calculated from the dependence of the collected charge ( $N_{coll}$ ) on the electric field ( $F$ ) in liquid Ar, accounting for the recombination effect using the following parameterization with the recombination coefficient  $k_{rec}$  [1, 3, 44]:

$$N_{coll} = N_i \cdot \frac{T_e \cdot \exp(-K_{att} \cdot C \cdot X)}{1 + k_{rec}/F}. \quad (3.2)$$

Here in addition, both the electron transmission through the THGEM0 electrode ( $T_e = 99\%$ ) and the attachment of electrons drifting over the distance  $X$  to electronegative impurities (with concentration  $C$ ) were taken into account, using the attachment coefficient  $K_{att}$ . The latter was taken as [44]:

$$K_{att} = 0.95/F^{0.8}, \quad (3.3)$$

where  $K_{att}$  is expressed in  $(\text{ppm}\cdot\text{mm})^{-1}$  and  $F$  in  $\text{kV}/\text{cm}$ . The recombination coefficient is a function of the energy and is described by the following equation (see Fig. 4 in [14]):

$$k_{rec}[\text{V}/\text{cm}] = 485 + 47000/E[\text{keV}]. \quad (3.4)$$

The collected charge in pure Ar was fitted by (3.2), where the primary ionization charge ( $N_i$ ) and impurity concentration ( $C$ ) were used as free parameters: see Fig. 6. The obtained impurity concentration amounted to about  $2 \pm 0.8$  ppb, which corresponds to electron lifetime of  $150 \pm 60 \mu\text{s}$  at a drift field of  $200 \text{ V}/\text{cm}$ .

The obtained primary ionization charge in measurements with pulsed X-rays amounted to  $7.9 \times 10^6 e^-$ , which corresponds to the energy deposition of  $186 \text{ MeV}$ .

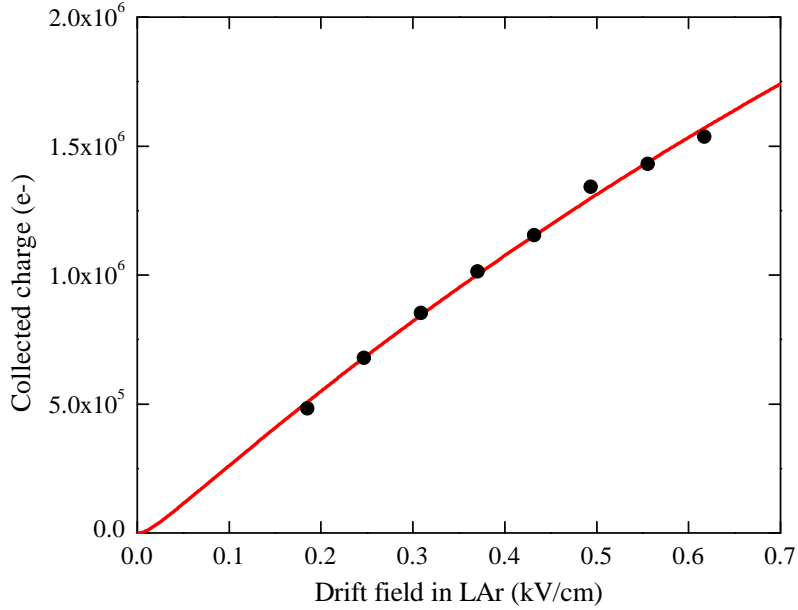


**Figure 6.** Collected charge in pure liquid Ar as a function of the drift field, obtained in the single-phase mode. Red curve is the fit by (3.2), where  $N_i$  and  $C$  are free parameters.

### 3.4 Absolute visible light yield

The absolute light yield is defined as the number of emitted photons per 1 MeV of deposited energy, i.e. it is equal to the ratio of the photoelectron number to the deposited energy and to the photon-to-photoelectron conversion efficiency ( $PCE$ ):  $Y = N_{PE}/E_{dep}/PCE$ . The conversion efficiency is defined as  $PCE = \varepsilon \langle PDE \rangle$ . Here  $\varepsilon$  is the photon collection efficiency, calculated using Monte Carlo simulation, and  $\langle PDE \rangle$  is the SiPM PDE or PMT QE averaged over the emission spectrum of liquid Ar taken from either [10] or [12] and appropriately convoluted with the acrylic transmittance spectrum (see Fig. 2).

The light yield thus obtained is shown in table 1 for pure liquid Ar at the maximum electric field and wavelength range of 400-1000 nm. The error in the recorded photoelectron number was about 10% for X-rays (mainly due to calibration uncertainty) and about 15% for alpha-particle source (due to calibration uncertainty and low photoelectron statistics). The systematic error in deposited

**Table 1.** Absolute light yield induced by pulsed X-rays and alpha particles, recorded by SiPM matrix and PMTs and calculated in the wavelength range of 400-1000 nm using emission spectrum from either [10] or [12].

Source	Spectral device	Light yield (photon/MeV) for spectrum of	
		[10]	[12]
25 keV X-rays	PMTs	$71 \pm 14$	$121 \pm 24$
	SiPM matrix	$212 \pm 42$	$187 \pm 37$
5.5 MeV $\alpha$	PMTs	$43 \pm 9$	$107 \pm 22$
	SiPM matrix	$98 \pm 20$	$87 \pm 17$

energy was about 15% for X-rays, while for alpha particles it was insignificant. The PCE error was about 10% and is mainly due to uncertainty in QE and PDE of PMTs and SiPMs, respectively. Using the root mean square formula to sum the mentioned factors, the error in the absolute light yields turned out to be about 20%, regardless of the photon detector and radiation source. Interestingly, the yield is almost independent of which emission spectrum is used, in particular for SiPM matrix data, which indicates that the results are weakly dependent on the shape of the spectrum if the latter is sufficiently flat (as in our case). Therefore in the following, we use the light yields obtained with the SiPM matrix rather than those of PMTs. The resulting light yield in pure liquid Ar was taken as the average between the yields for the two emission spectra (for that of [10] and [12]): it amounted to  $200 \pm 50$  photon/MeV and  $92 \pm 23$  photon/MeV for pulsed X-rays and alpha particles, respectively.

### 3.5 Comparison with the previous results

Table 2 shows a compilation of the results on light emission in liquid Ar in the visible and NIR range. Let us compare these to those of the present work.

First of all, the results of the present work confirm those of our (Novosibirsk group) previous works [6–8]. Indeed, visible-light emission in liquid Ar was observed there in the range of 400-1000 nm, using the same X-ray tube. The signal pulse shapes were analyzed on a large time scale, of about 50  $\mu$ s, resulting in that the fast and slow components were not distinguishable, unlike the measurements of the present work (see Fig. 4). Using the spectrum from [10], the absolute light yield was determined: it amounted to  $510 \pm 90$  photon/MeV, which is consistent with that of the present work within a factor of 2.5. Similarly to the present work, almost no field dependence was observed.

It should be remarked that in the present work, in measurements with X-rays the signal had the fast ( $\tau_f < 100$  ns) and slow ( $\tau_s \sim 1$   $\mu$ s) components with approximately the same contribution. On the other hand, in measurements with alpha particles, only the fast component was observed, which may indicate on somewhat different emission mechanisms when irradiated by X-rays and alpha particles.

The present results are also in compliance with those of [11, 13] (FNAL group): light emission in the NIR in liquid Ar were observed there in the range of 715-900 nm, when irradiated with

**Table 2.** Compilation of the results on light emission in liquid Ar in the visible and NIR range.

Reference	Excitation source	Electric field (kV/cm)	Spectrum range (nm)	Light yield in visible and NIR range (photon/MeV)	Comments
[9, 10]	12 keV e <sup>-</sup>	0	300-1000	Observed	Spectrum measured
[6–8]	25 keV X-rays	0-30	400-1000	510 ± 90	Field independent
[45] [46]	12 keV e <sup>-</sup>	0	500-1000	Not observed Observed in NIR	
[11]	511 keV γ-rays	0	715-900	Observed	$\tau_f < 100$ ns $\tau_s \approx 2 - 4$ μs Field independent
[12]	HV breakdown	≤200	400-800	Observed	Spectrum measured
This work	25 keV X-rays	0-0.62	400-1000	200 ± 50	$\tau_f < 100$ ns $\tau_s = 1 \pm 0.3$ μs
[28]	5.3 MeV α	0	300-650	Not observed	<10 ph./MeV
[47]	10 MeV protons	0	300-1000	Observed	Spectrum measured
[13]	5.4 MeV α	0	715-900	Observed	
This work	5.5 MeV α	0.3-0.62	400-1000	92 ± 23	$\tau_f < 100$ ns No slow comp. Field independent

511 keV gamma-rays and 5.4 MeV alpha particles. Analyzing the pulse shapes presented in [11], one may conclude that the authors observed the fast ( $\tau_f < 100$  ns) and slow ( $\tau_s = 2 - 4$  μs) signal components, similarly to that of the present work.

The third group that observed visible-light emission in liquid Ar was that of [12]: electroluminescence was observed at 400-800 nm, induced by high-voltage electrical breakdown. The spectrum of the emission continuum was measured.

The results of the fourth group (Munich group) are somewhat contradictory. On one hand, an emission continuum in the visible and NIR range was observed in liquid Ar at 300-900 nm [9, 10, 47], in addition to excimer scintillations in the VUV, when irradiated with 12 keV electron and 10 MeV proton beams. The spectrum of the continuum was measured. Moreover, in [47] it was

hypothesized that this emission continuum could be explained by the bremsstrahlung effect. On the other hand, later the same group [45, 46] first claimed that the continuum observed in [9, 10, 47] “was an artifact due to the normalization of the spectrum with the response function of the spectrometer used for that spectral region” [45], but then again reported on observation of emission in the NIR [46]. Therefore, we tend to think that this group did observe such visible-light emission and therefore it is justified to use their spectrum in the analysis of the results.

Finally, the fifth group [28] did not observe photon emission in liquid Ar in the visible range, when irradiated with 5.3 MeV alpha particles, in contradiction with the results of our and FNAL groups: the light yield was estimated to be less than 10 photon/MeV, which is an order of magnitude lower than that of the present work.

## 4 Measurements with liquid argon doped with methane

### 4.1 Pulse-shape analysis

Fig. 7 shows the averaged pulse shapes of the S1 signals from PMTs and SiPM matrix, induced by pulsed X-rays, obtained in liquid Ar and liquid mixture Ar+CH<sub>4</sub> (140 ppm) at zero electric field. One can see that even a small amount of CH<sub>4</sub> dopant (140 ppm) resulted in disappearance of the slow component observed in pure liquid Ar. With further increase of the CH<sub>4</sub> content, up to 10%, the pulse shape did not change. Also, the pulse shape did not depend on the electric field.

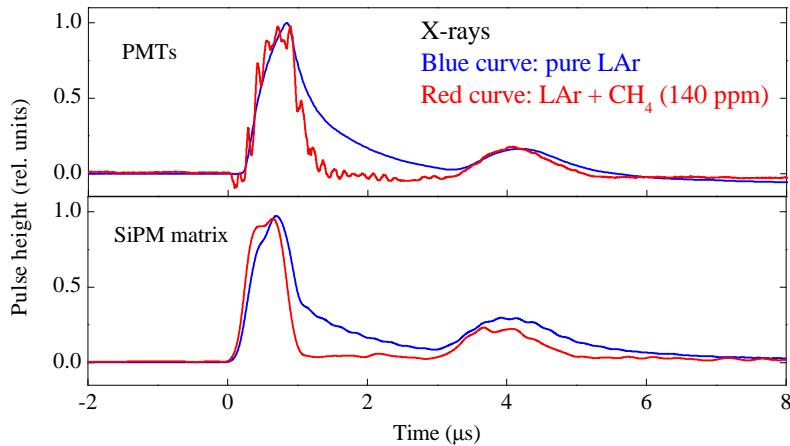


**Figure 7.** Averaged pulse shapes of S1 signals, induced by pulsed X-rays, obtained in the two-phase mode in pure liquid Ar and liquid mixture Ar+CH<sub>4</sub> (140 ppm) at zero electric field, recorded by SiPM matrix and PMTs. All the pulse heights are normalized to the maximum.

Fig. 8 shows the averaged pulse shapes of both S1 and S2 signals, induced by alpha particles and obtained in the two-phase mode in pure liquid Ar and its mixtures with CH<sub>4</sub> (140 ppm, 0.1% and 1%) at the maximum electric field. The maximum electric field was needed to provide the efficient trigger using the S2 signal, as discussed in section 2. Accordingly, the S1 pulse width would be mostly defined by the jitter of the S2 pulse trigger, if the visible-light emission is really fast. We will see that this is indeed the case.

It is seen that when increasing the CH<sub>4</sub> content the S2 signal became faster, its slow component quickly disappearing (see [40] for explanation of the S2 slow component). In addition, its amplitude

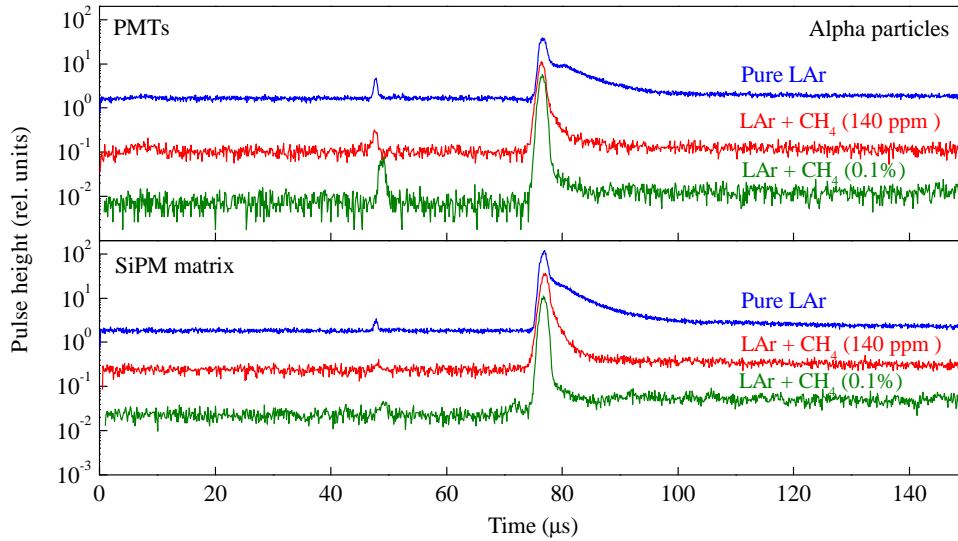


**Figure 8.** Averaged pulse shapes of S1 and S2 signals, induced by alpha particles, obtained in the two-phase mode in pure liquid Ar and liquid mixtures Ar+CH<sub>4</sub> (140 ppm, 0.1%) at maximum electric field ( $F_d = 0.62$  kV/cm,  $F_{EL} = 7.8$  kV/cm), recorded by SiPM matrix and PMTs. The pulse heights are proportional to the number of photoelectrons of S2 signal to highlight the difference in S2 pulse shapes and S2 yields.

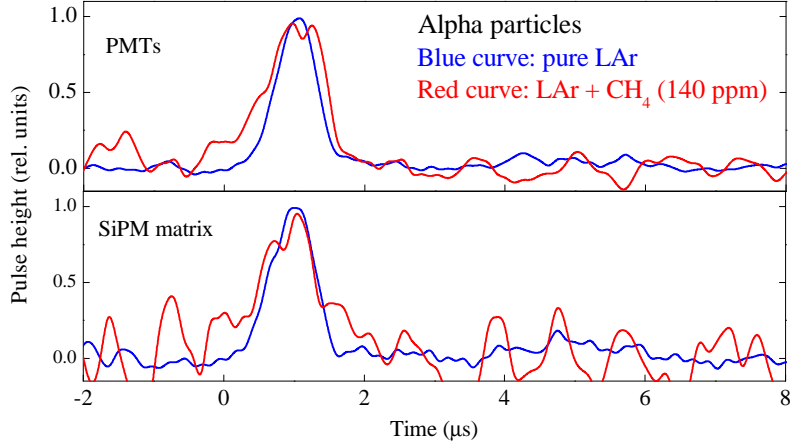
and drift time (time difference between S1 and S2) decreased. The estimated drift times in liquid Ar doped with methane are in good agreement with the data reported elsewhere (see fig. 13).

Fig. 9 shows the enlarged view of the S1 signals from Fig. 8 in pure liquid Ar and its mixture with CH<sub>4</sub> (140 ppm). One can see that in both cases the S1 pulse shapes look the same, containing only the fast component. This may indicate on the common origin of the fast component in visible-light emission in pure liquid Ar and in its mixtures with CH<sub>4</sub>. Here the pulse shape of the fast component is defined mostly by the S2 signal jitter, which was much larger than the characteristic time of the NBrS emission in pure Ar and CH<sub>4</sub>-doped Ar. That is why the S1 pulse shape was not sensitive to doping Ar with CH<sub>4</sub>.

## 4.2 Photoelectron and light yields

To calculate the photoelectron yield in argon-methane mixtures, the photoelectron number was calculated in a 10  $\mu$ s interval, similarly to that of pure Ar. Figs. 10 and 11 show the relative photoelectron yield of visible-light emission induced by pulsed X-rays and alpha particles in liquid Ar mixtures with CH<sub>4</sub> as a function of the CH<sub>4</sub> content. One can see that the data obtained with PMTs and SiPM matrix are in reasonable agreement, within a factor of 1.5 on average, despite the fact that PMTs and SiPMs are sensitive in different spectral ranges (see Fig. 2). This fact indicates that the spectrum of visible-light emission is rather flat and that its shape does not significantly change when CH<sub>4</sub> dopant is added.

The absolute light yield is also shown in the figures 10 and 11 (right scale), obtained similarly to that of pure Ar, i.e. using SiPM-matrix data and averaged over the two emission spectra taken from [10, 12]. Here the visible-light emission spectra of [10, 12] for pure liquid Ar were used since



**Figure 9.** Averaged pulse shapes of S1 signals, induced by alpha particles, obtained in the two-phase mode in pure liquid Ar and liquid mixture Ar+CH<sub>4</sub> (140 ppm) at the maximum electric field ( $F_d = 0.62$  kV/cm,  $F_{EL} = 7.8$  kV/cm), recorded by SiPM matrix and PMTs. All the pulse heights are normalized to the maximum.

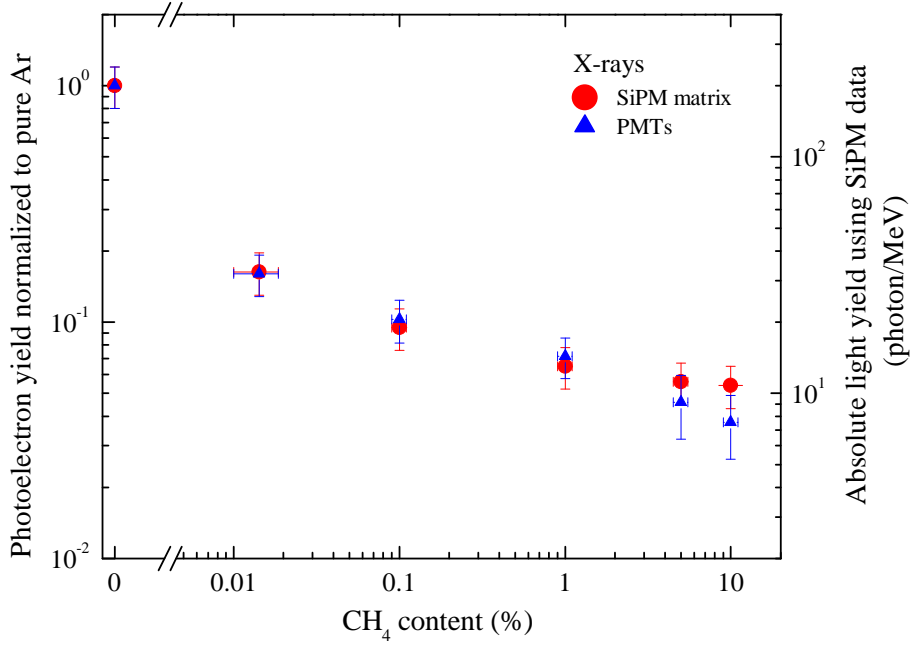


**Figure 10.** Relative photoelectron yield of visible-light emission, induced by pulsed X-rays and measured in the two-phase mode in liquid Ar mixtures with CH<sub>4</sub>, as a function of the CH<sub>4</sub> molar content at zero electric field, recorded by SiPM matrix and PMTs. Also shown is the absolute light yield obtained using SiPM-matrix data and averaged over two emission spectra from refs. [10, 12] (right scale, relevant to the SiPM-matrix data points).

they are the only ones available and since those for argon-methane mixtures are not available in the literature. Such a treatment is allowed due to the following points. Firstly, one could see in Section 3.4 that the photon yield was almost independent of the spectrum shape, in particular due to the

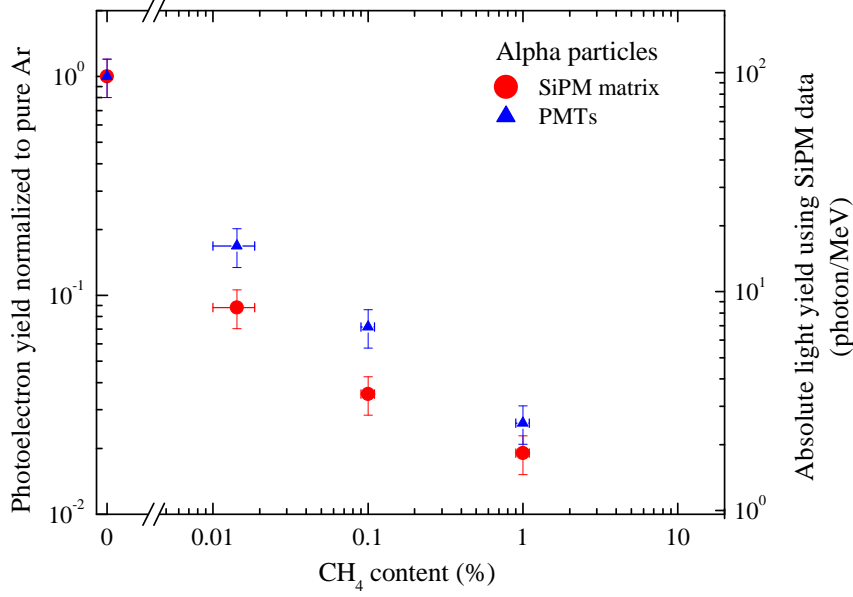


**Figure 11.** Relative photoelectron yield of visible-light emission, induced by alpha particles and measured in the two-phase mode in liquid Ar mixtures with CH<sub>4</sub>, as a function of the CH<sub>4</sub> molar content at the maximum electric field ( $F_d = 0.62$  kV/cm,  $F_{EL} = 7.8$  kV/cm), recorded by SiPM matrix and PMTs. Also shown is the absolute light yield obtained using SiPM-matrix data and averaged over two emission spectra from [10, 12] (right scale, relevant to the SiPM-matrix data points).

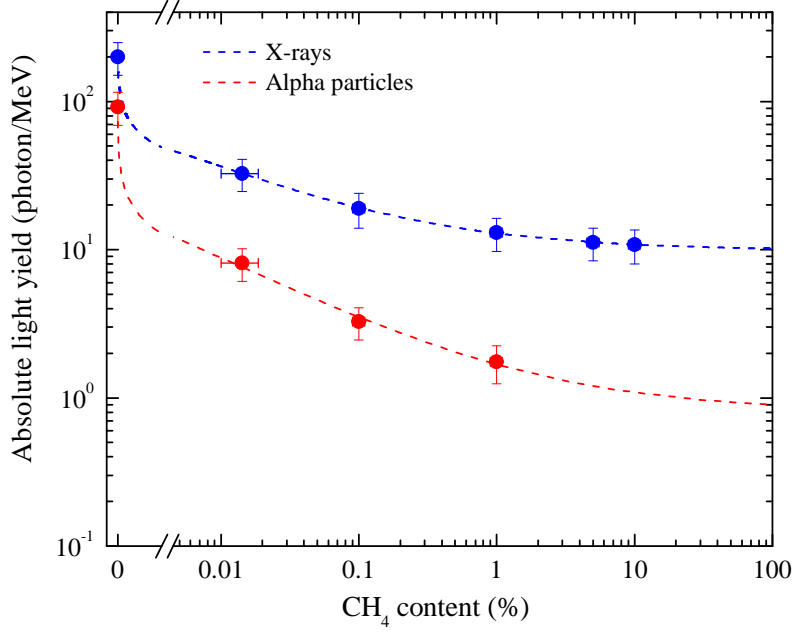
fact that the spectra used are rather flat (see Fig. 2). Secondly, if the spectrum is indeed determined by the NBrS effect, its shape should not depend much on which species the electron is scattered on (Ar or CH<sub>4</sub>), since numerous NBrS spectra of various origins presented in the literature look very flat and therefore very similar to each other [15, 22, 23]. On the other hand, the presence of CH<sub>4</sub> dopant can affect the energy distribution of delta electrons and hence the properties of the NBrS emission produced by them, but our experimental procedures were not sensitive to such changes in the emission spectrum.

Fig. 12 and table 3 summarize the results on the absolute photon yield of visible-light emission in pure liquid Ar and its mixtures with CH<sub>4</sub>. Looking at these results one may conclude the following.

For X-rays, the absolute photon yield of visible-light emission in pure liquid Ar is about 200 photon/MeV. In liquid argon doped with methane, the photon yield dropped down significantly, by about an order of magnitude at a CH<sub>4</sub> content varying from 0.01 to 1%, and then almost did not change when further increasing the content up to 10%, reaching a plateau at about 10 photon/MeV.

For alpha particles, the photon yield is reduced compared to that of X-rays, the reduction factor changing from 2 in pure liquid Ar (90 photon/MeV) to 7 at 1% CH<sub>4</sub> content. Nevertheless, the CH<sub>4</sub> content dependence looks very similar to that of X-rays: there is an obvious trend towards a plateau, but due to the lack of data above 1% it is not completed (at higher CH<sub>4</sub> contents the S2 signal was too weak to provide the trigger). Extrapolation of the data gives a plateau value of about 1 photon/MeV for the photon yield.

Such a characteristic dependence on the CH<sub>4</sub> content can be qualitatively explained in the



**Figure 12.** Absolute light yield, induced by pulsed X-rays at zero electric field and by alpha particles at the maximum electric field ( $F_d = 0.62$  kV/cm,  $F_{EL} = 7.8$  kV/cm), in liquid Ar mixtures with CH<sub>4</sub> as a function of the CH<sub>4</sub> content. The results were obtained using SiPM-matrix data and averaged over two emission spectra from refs. [10, 12]. The curves are the sigmoidal function fit to the data points.

framework of NBrS mechanism. Indeed, the NBrS intensity is proportional to the energy of primary ionization electrons (see formula 4 in [15]). When adding CH<sub>4</sub> to liquid Ar, the electron energy decreases with the CH<sub>4</sub> content due to enhancement of inelastic collisions with CH<sub>4</sub> molecules, until they fully dominate at higher contents, thus producing a plateau in CH<sub>4</sub> content dependence.

Finally, with a CH<sub>4</sub> content of 1% (the minimum required for a compact neutron veto detector), the absolute photon yield of visible-light emission for X-rays is about 13 photon/MeV. This value seems to be too small for the effective detection of gamma-rays accompanying neutron capture on argon and hydrogen. Accordingly, liquid Ar doped with CH<sub>4</sub> can hardly be used as a scintillating medium for neutron veto detectors. On the other hand, it might be considered to be used in scintillation hadron calorimetry, since methane allows to compensate the calorimeter and thus increase its energy resolution.

## 5 Conclusions

In this work the properties of visible-light emission in pure liquid argon and its mixtures with methane have been systematically studied, using cryogenic PMTs and a SiPM matrix. The light yield in pure liquid argon was measured to be about 200 and 90 photon/MeV for X-rays and alpha particles respectively, in the wavelength range of 400-1000 nm.

In liquid argon doped with methane the light yield dropped down significantly, by about an order of magnitude at a methane molar content varying from 0.01 to 1%, and then almost did not

**Table 3.** Absolute light yield in pure liquid Ar and its mixtures with CH<sub>4</sub> at 400-1000 nm induced by pulsed X-rays and alpha particles at zero and maximum electric field ( $F_d = 0.62$  kV/cm,  $F_{EL} = 7.8$  kV/cm) respectively.

Liquid mixture	Light yield (photon/MeV)	
	Pulsed X-rays (zero field)	Alpha particles ( $F_d = 0.62$ kV/cm)
LAr (100%)	200±50	92±23
LAr + CH <sub>4</sub> (140 ppm )	32±8	8.2±2.0
LAr + CH <sub>4</sub> (0.1% )	19±5	3.3±0.8
LAr + CH <sub>4</sub> (1%)	13.0±3.3	1.8±0.5
LAr + CH <sub>4</sub> (5%)	11.3±2.8	-
LAr + CH <sub>4</sub> (10%)	11.1±2.8	-

change when further increasing the methane content up to 10%, reaching a plateau at about 10 photon/MeV for X-rays.

For alpha particles, the light yield is reduced compared to that of X-rays, the reduction factor changing from 2 in pure liquid argon to 7 at 1% methane molar content.

Due to such a small light yield, liquid argon doped with methane can hardly be used as working medium for neutron veto detectors.

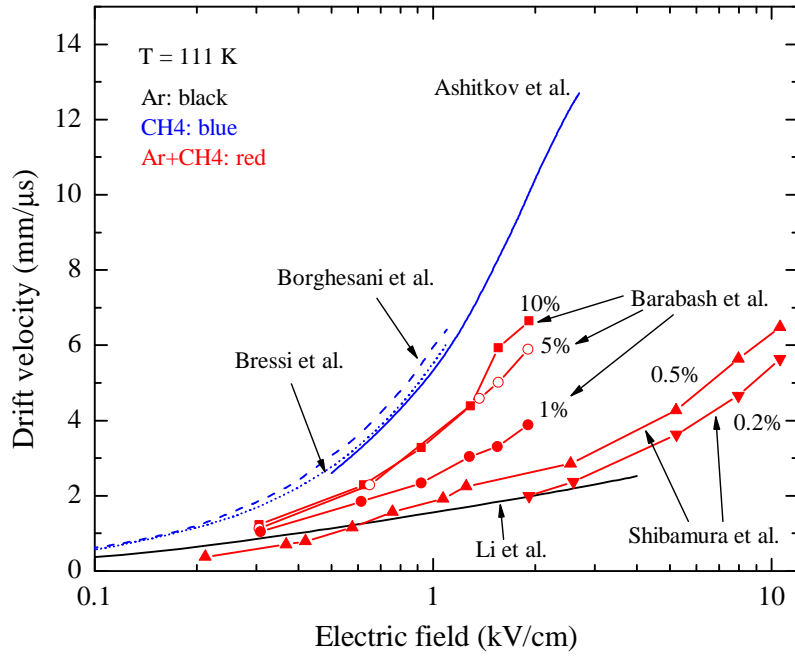
Based on the observed properties of visible-light emission in both pure and methane-doped liquid argon, we propose that it is due to neutral bremsstrahlung of primary ionization electrons.

## A Doping liquid argon with methane: drift velocity and charge yield

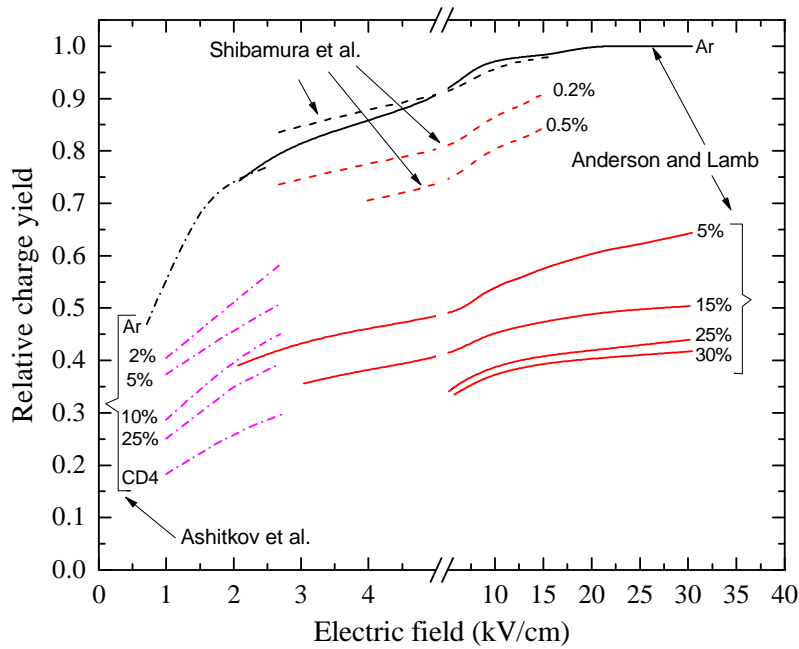
In this Appendix a compilation of data on drift velocity and charge yield in liquid Ar, liquid CH<sub>4</sub> and their mixtures is presented.

Fig. 13 shows the electron drift velocity as a function of the electric field in these media. Since the drift velocity depends on the liquid temperature as  $T^{-3/2}$  over a wide temperature range [48–50], all data are reduced to the same temperature, of 111 K, for comparison under the same conditions. The temperature of 111 K was chosen to minimize the interpolation error and because it corresponds to the boiling point of methane at atmospheric pressure. One can see that the electron drift velocity substantially increases with the CH<sub>4</sub> content.

Figs. 14 and 15 show the dependence of the relative charge yield, from tracks of relativistic electrons and alpha particles respectively, on the electric field in liquid Ar, liquid methane/deuteromethane and their mixtures. The relative charge yield is defined as the ratio of the charge collected at a given electric field to the maximum charge collected from tracks of relativistic electrons at the infinite electric field. Here the equation (3.2) with  $T_e = 100\%$  and  $C = 0$  was used to fit the charge yield as a function of the electric field. It is seen that the charge yield substantially decreases with the methane content.



**Figure 13.** Electron drift velocity as a function of the electric field in liquid Ar, liquid CH<sub>4</sub> and their mixtures taken from Ashitkov et al. [51], Barabash et al. [52], Borghesani et al. [53], Bressi et al. [54], Li et al. [50], Shibamura et al. [55]. The drift velocity values are reduced to the same temperature, of 111 K, using  $T^{-3/2}$  dependence [48–50].



**Figure 14.** Relative charge yield from tracks of relativistic electrons as a function of the electric field in liquid Ar and its mixtures with CH<sub>4</sub>/CD<sub>4</sub> taken from Anderson and Lamb [56] (maximum electron energy of 3.5 MeV), Ashitkov et al. [51] (1.06 MeV Compton electrons), Shibamura et al. [55] (0.976 MeV electrons), normalized to the maximum collected charge in liquid Ar at the infinite electric field.

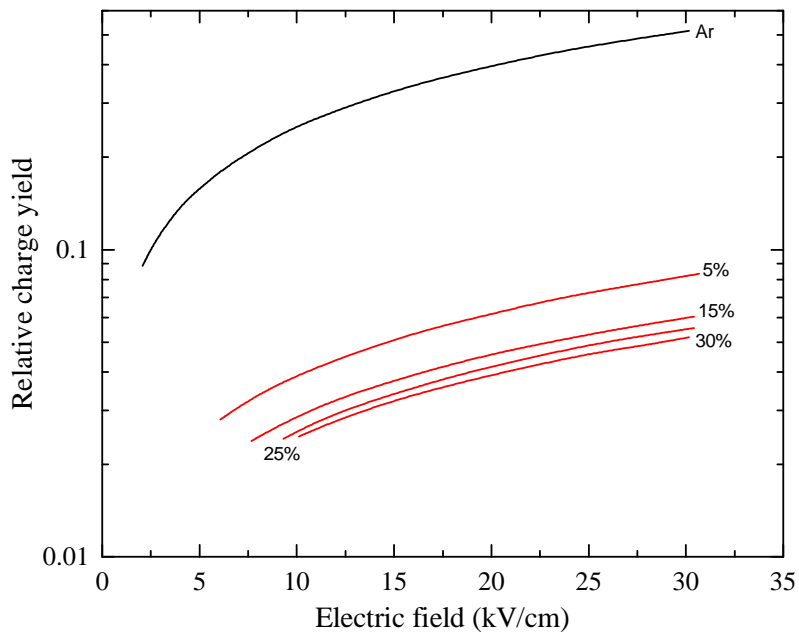


**Figure 15.** Relative charge yield from tracks of 5.5 MeV alpha particles as a function of the electric field in liquid Ar and its mixtures with CH<sub>4</sub> at CH<sub>4</sub> content of 5%, 15%, 25% and 30%. The data are taken from Anderson and Lamb [56], normalized to the maximum charge collected from tracks of relativistic electrons in liquid Ar at the infinite electric field.

## Acknowledgments

This work was supported in part by Russian Science Foundation (project no. 20-12-00008). It was done within the R&D program of the DarkSide-20k experiment.

## References

- [1] V. Chepel and H. Araujo, *Liquid noble gas detectors for low energy particle physics*, *J. Instrum.* **8** (2013) R04001.
- [2] K. Majumdar and K. Mavrokoridis, *Review of liquid argon detector technologies in the neutrino sector*, *Appl. Sci.* **15** (11) 2455.
- [3] D. Y. Akimov, A. I. Bolozdynya, A. F. Buzulutskov and V. Chepel, *Two-phase emission detectors*, *World Scientific, New Jersey* (2021) .
- [4] A. Buzulutskov, *Electroluminescence and electron avalanching in two-phase detectors*, *Instrum.* **4** (2020) 16.
- [5] A. Buzulutskov, *Photon emission and atomic collision processes in two-phase argon doped with xenon and nitrogen*, *Europhys. Lett.* **117** (2017) 39002.
- [6] A. Buzulutskov et al., *Infrared scintillation yield in gaseous and liquid argon*, *Europhys. Lett.* **94** (2011) 52001.
- [7] A. Bondar et al., *Study of infrared scintillations in gaseous and liquid argon. Part I: methodology and time measurements*, *J. Instrum.* **7** (2012) P06015.
- [8] A. Bondar et al., *Study of infrared scintillations in gaseous and liquid argon. Part II: light yield and possible applications*, *J. Instrum.* **7** (2012) P06014.
- [9] T. Heindl et al., *The scintillation of liquid argon*, *Europhys. Lett.* **91** (2010) 62002.
- [10] T. Heindl et al., *Table-top setup for investigating the scintillation properties of liquid argon*, *J. Instrum.* **6** (2011) P02011.
- [11] T. Alexander et al., *Near-infrared scintillation of liquid argon*, *J. Instrum.* **11** (2016) C03010.
- [12] M. Auger et al., *On the electric breakdown in liquid argon at centimeter scale*, *J. Instrum.* **11** (2016) P03017.
- [13] C. O. Escobar et al., *Near-infrared scintillation of liquid argon: recent results obtained with the NIR facility at Fermilab*, *J. Instrum.* **13** (2018) C03031.
- [14] A. Bondar et al., *Observation of primary scintillations in the visible range in liquid argon doped with methane*, *J. Instrum.* **15** (2020) C06064.
- [15] A. Buzulutskov et al., *Revealing neutral bremsstrahlung in two-phase argon electroluminescence*, *Astropart. Phys.* **103** (2018) 29.
- [16] A. Bondar et al., *Neutral bremsstrahlung in two-phase argon electroluminescence: further studies and possible applications*, *Nucl. Instrum. Methods Phys. Res. A* **958** (2020) 162432.
- [17] M. Kimura et al., *Measurements of argon-scintillation and -electroluminescence properties for low mass WIMP dark matter search*, *J. Instrum.* **15** (2020) C08012.
- [18] T. Takeda et al., *Study of luminescence mechanism by neutral bremsstrahlung in gaseous argon*, *J. Instrum.* **15** (2020) C03007.

- [19] K. Aoyama et al., *Measurement of emission spectrum for gaseous argon electroluminescence in visible light region from 300 to 600 nm*, *Nucl. Instrum. Methods Phys. Res. A* **1025** (2022) 166107.
- [20] C. E. Aalseth et al., *SiPM-matrix readout of two-phase argon detectors using electroluminescence in the visible and near infrared range*, *Eur. Phys. J. C* **81** (2021) 153.
- [21] C. A. O. Henriques et al., *Neutral bremsstrahlung emission in xenon unveiled*, *Phys. Rev. X* **12** (2022) 021005.
- [22] E. Borisova and A. Buzulutskov, *Neutral bremsstrahlung and excimer electroluminescence in noble gases and its relevance to two-phase dark matter detectors*, *Eur. Phys. J. C* **81** (2021) 1128.
- [23] E. Borisova and A. Buzulutskov, *Neutral bremsstrahlung electroluminescence in noble liquids*, *Europhys. Lett.* **137** (2022) 24002.
- [24] P. Amedo et al., *Neutral bremsstrahlung in TPCs*, *J. Instrum.* **17** (2022) C02017.
- [25] P. Agnes et al., *First results from the DarkSide-50 dark matter experiment at Laboratori Nazionali del Gran Sasso*, *Phys. Lett. B* **743** (2015) 456–466.
- [26] P. Agnes et al., *The veto system of the DarkSide-50 experiment*, *J. Instrum.* **11** (2016) P03016.
- [27] C. Galbiati, private communication.
- [28] B. J. P. Jones et al., *The effects of dissolved methane upon liquid argon scintillation light*, *J. Instrum.* **8** (2013) P12015.
- [29] H. Keller-Rudek et al., *The MPI-Mainz UV/VIS Spectral Atlas of Gaseous Molecules of Atmospheric Interest*, *Earth Syst. Sci. Data* **5** (2013) 365–373.
- [30] I. Al Samarai et al., *Molecular bremsstrahlung radiation at GHz frequencies in air*, *Phys. Rev. D* **93** (2016) 052004.
- [31] Pfeiffer Vacuum. <https://www.pfeiffer-vacuum.com>.
- [32] [www.spectron.de](http://www.spectron.de).
- [33] <https://okba.ru/product/datchik-kisloroda/gazoanalizator-svet/>.
- [34] A. Breskin et al., *A concise review on THGEM detectors*, *Nucl. Instrum. Methods Phys. Res. A* **598** (2009) 107.
- [35] A. Bondar et al., *Characterization of photo-multiplier tubes for the cryogenic avalanche detector*, *J. Instrum.* **10** (2015) P10010.
- [36] [www.hamamatsu.com](http://www.hamamatsu.com).
- [37] A. Otte et al., *Characterization of three high efficiency and blue sensitive silicon photomultipliers*, *Nucl. Instrum. Methods Phys. Res. A* **846** (2017) 106.
- [38] A. Lyashenko et al., *Measurement of the absolute quantum efficiency of Hamamatsu model R11410-10 photomultiplier tubes at low temperatures down to liquid xenon boiling point*, *J. Instrum.* **9** (2014) P11021.
- [39] A. Bondar et al., *X-ray ionization yields and energy spectra in liquid argon*, *Nucl. Instrum. Methods Phys. Res. A* **816** (2016) 119.
- [40] A. Bondar et al., *Observation of unusual slow components in electroluminescence signal of two-phase argon detector*, *J. Instrum.* **15** (2020) C06064.
- [41] P. Agnes et al., *Measurement of the liquid argon energy response to nuclear and electronic recoils*, *Phys. Rev. D* **97** (2018) 112005.

- [42] M. J. Berger et al., *Stopping-Power and Range Tables for Electrons, Protons, and Helium Ions*, .
- [43] M. Miyajima et al., *Average energy expended per ion pair in liquid argon*, *Phys. Rev. A* **9** (1974) 1438.
- [44] E. Aprile et al., *Noble gas detectors*, Wiley-VCH, Weinheim, 2006, and references therein (2006) .
- [45] A. Neumeier et al., *Intense infrared scintillation of liquid Ar-Xe mixtures*, *Europhys. Lett.* **106** (2014) 32001.
- [46] A. Neumeier et al., *Intense vacuum ultraviolet and infrared scintillation of liquid Ar-Xe mixtures*, *Europhys. Lett.* **109** (2015) 12001.
- [47] M. Hofmann et al., *Ion-beam excitation of liquid argon*, *Eur. Phys. J. C* **73** (2013) 2618.
- [48] M. H. Cohen and J. Lekner, *Theory of Hot Electrons in Gases, Liquids, and Solids*, *Phys. Rev.* **158** (1967) 305.
- [49] J. M. L. Engels and A. J. M. Van Kimmenade, *The motion of excess electrons in liquid mixtures of methane and argon*, *Chem. Phys. Lett.* **15** (1977) 451–454.
- [50] Y. Li et al., *Measurement of longitudinal electron diffusion in liquid argon*, *Nucl. Instrum. Methods Phys. Res. A* **816** (2016) 160–170.
- [51] V. D. Ashitkov et al., *A study of the electronic properties of liquid argon–deuteromethane mixtures*, *Instrum. Exp. Tech.* **44** (2001) 626.
- [52] A. S. Barabash et al., *Investigation of some characteristics of a liquid methane pulsed ionization chamber*, *Nucl. Instrum. Methods* **186** (1981) 525.
- [53] A. F. Borghesani et al., *Electron mobility in high purity liquid CH<sub>4</sub>*, *Phys. Lett. A* **160** (1991) 483.
- [54] G. Bressi et al., *Preliminary results on the feasibility of a liquid methane detector for fast neutrons*, *Nucl. Instrum. Methods Phys. Res. A* **300** (1991) 321.
- [55] E. Shibamura et al., *Drift velocities of electrons, saturation characteristics of ionization and W-values for conversion electrons in liquid argon, liquid argon-gas mixtures and liquid xenon*, *Nucl. Instrum. Methods* **131** (1975) 249.
- [56] D. F. Anderson and D. C. Lamb, *Saturation effects in liquid argon doped with methane*, *Nucl. Instrum. Methods Phys. Res. A* **265** (1988) 440.